Synaptic Efficacy and the Transmission of Complex Firing Patterns Between Neurons

PHILIPPE FAURE, DANIEL KAPLAN, AND HENRI KORN
Biologie Cellulaire et Moléculaire du Neurone (Institut National de la Santé et de la Recherche Médicale U261), Institut Pasteur, 75724 Paris Cedex 15, France

Received 15 February 2000; accepted in final form 25 July 2000

Faure, Philippe, Daniel Kaplan, and Henri Korn. Synaptic efficacy and the transmission of complex firing patterns between neurons. *J Neurophysiol* 84: 3010–3025, 2000. In central neurons, the summation of inputs from presynaptic cells combined with the unreliability of synaptic transmission produces incessant variations of the membrane potential termed synaptic noise (SN). These fluctuations, which depend on both the unpredictable timing of afferent activities and quantal variations of postsynaptic potentials, have defied conventional analysis. We show here that, when applied to SN recorded from the Mauthner (M) cell of teleosts, a simple method of nonlinear analysis reveals previously undetected features of this signal including hidden periodic components. The phase relationship between these components is compatible with the notion that the temporal organization of events comprising this noise is deterministic rather than random and that it is generated by presynaptic interneurons behaving as coupled periodic oscillators. Furthermore a model of the presynaptic network shows how SN is shaped both by activities in incoming inputs and by the distribution of their synaptic weights expressed as mean quantal contents of the activated synapses. In confirmation we found experimentally that long-term tetanic potentiation (LTP), which selectively increases some of these synaptic weights, permits oscillating temporal patterns to be transmitted more effectively to the postsynaptic cell. Thus the probabilistic nature of transmitter release, which governs the strength of synapses, may be critical for the transfer of complex timing information within neuronal assemblies.

INTRODUCTION

The nature of the neural code has led to much speculation (for a review, see Buzsaki et al. 1994; Eggermont 1998; Fuji et al. 1996). For example it has been proposed (Hebb 1949; Hopfield 1995; Perkel and Bullock 1968; Von der Malsburg 1981) that the coding of information in the CNS emerges from different firing patterns. Such codes may include the rate of action potentials (Georgopoulos et al. 1986; Shadlen and Newsome 1998), well-defined synchronous activities of the "gamma" type (40 Hz) particularly during binding (Singer 1993), and more complex temporal organization of firing in large networks (Nicolelis et al. 1995; Riehle et al. 1997).

Relevant to the present study, it has been suggested that chaos, found in several areas of the CNS (Pei and Moss 1996; Schiff et al. 1994), may also contribute to the neuronal code (Skarda and Freeman 1987, 1990; So et al. 1998; van Vreeswijk and Sompolinski 1996). But the validation of this hypothesis requires a demonstration that deterministic patterns can be, and are effectively, transmitted along neuronal chains.

This issue faces numerous difficulties, particularly in in vivo preparations, due to the variability of the ongoing activity in neurons called synaptic noise (SN) (Brock et al. 1952). This noise has been first attributed to a "random synaptic bombardment" of the recorded cells. Except for an early claim (Calvin and Stevens 1967) and some recent reports (Arieli et al. 1995 1996), the view according to which SN degrades neuronal functions has remained prevalent over the years (for a review see Ferster 1996). More important, this process has been commonly assumed to be stochastic (Calvin and Stevens 1967; Shadlen and Newsome 1998; Softky and Koch 1993), and it has been most often modeled as such (Mainen and Sejnowski 1995; Stevens and Zador 1998). Therefore recent studies on this intriguing phenomenon have mostly concentrated on whether or not, and in which conditions, such a Poisson process contributes to the variability of neuronal firing (Shadlen and Newsome 1994, 1995; Softky 1995). However, the renewed interest in SN leaves open the question of whether specific information about the state of firing of the presynaptic networks can be extracted from SN despite its random time appearance. The variability in both the amplitude and time of occurrence of the synaptic responses that build up SN precludes the sole use of conventional methods in solving this problem.

In this paper, we analyze the fine structure of SN in terms of timing and amplitude. SN was recorded intracellularly from the Mauthner (M) cell of teleosts, the command neuron of the adversive reaction to external stimuli (Zottoli 1977). Specifically we want to understand how SN reflects the state of the presynaptic networks and how synaptic junctions are involved in the transmission of this information. For this purpose, we examined physiological recordings using analytical tools based on nonlinear dynamics (for a review, see Abarbanel 1995; Schreiber 1999) already successfully applied to decipher the complexity of other neuronal systems (Guckenheimer and Rowat 1997; Pei and Moss 1996; Schiff et al. 1994). Our results indicate that, surprisingly, the fluctuating properties of synapses govern the degree to which complex activities in presynaptic networks are recapitulated postsynaptically and that this process is facilitated by a classical paradigm of learning.

Address for reprint requests: H. Korn, Biologie Cellulaire et Moléculaire du Neurone (INSERM U261), Institut Pasteur, 25 rue du Docteur Roux, 75724 Paris Cedex 15, France (E-mail: hkorn@pasteur.fr).

The costs of publication of this article were defrayed in part by the payment of page charges. The article must therefore be hereby marked "*advertisement*" in accordance with 18 U.S.C. Section 1734 solely to indicate this fact.

Part of this work has been presented in an abstract form (Faure and Korn 1998a).

METHODS

Electrophysiological recordings

In the M cell of teleosts, the command neuron of the escape reaction from adversive stimuli, SN is inhibitory and is generated by two groups of glycinergic interneurons (Fig. 1*A*) one of which is driven by auditory inputs (Faber and Korn 1978). This activity was recorded in vivo in a quiet auditory environment with KCl-filled microelectrodes in the M-cell lateral dendrite of anesthetized adult goldfish (*Carassius auratus*, $n = 14$) and zebrafish (*Brachydanio rerio*, $n = 16$) as described in Faure and Korn (1997). Because the inhibitory postsynaptic potential (IPSP) in the M cell is hard to detect as a potential change (Furshpan and Furukawa 1962), Cl− was iontophoretically injected through the recording microelectrode until large and stable full-sized depolarizing collateral IPSPs evoked by antidromic activation of the M axon (Faber and Korn 1982) were recorded. Thus the IPSPs comprising SN also appeared as depolarizing potentials (Fig. 1*B*, *top*). Recordings were digitized at 12 kHz and filtered at 3 kHz with a low-pass Bessel filter.

Data analysis

An approximation of the time derivative of the recorded signal was calculated using first differences. The peak amplitudes and times of occurrence of the resulting upstroke "spikes" constitute the signal that was subjected to further analysis. These spikes could be easily resolved against the background noise. The spike train was sieved by ignoring all events whose amplitudes fell below a specified threshold, θ. Thus the spike sequence submitted for further analysis depends on both the signal itself and the imposed threshold.

The derived trains were examined with several techniques. Interspike event histograms were constructed using a kernel-based density estimator (Parzen 1962). The power spectrum of the spike point process was estimated using the discrete-time Fourier transform of the 12 kHz signal set equal to 1 at the time of events and 0 elsewhere.

Nonlinear structures in the spike trains were examined graphically using return maps, also referred to as Poincaré maps (PMs) (Faure and Korn 1997, 1998b; Garfinkel et al. 1992). The PMs were constructed by scatter plotting each interval between two successive events $I(n + 1)$ versus the previous one $I(n)$. Note that in all maps presented in this report, each point corresponds to consecutive pairs of intervals (I_1, I_2) among three IPSPs. That is for the first data point of the illustrated series, $I(n) = I_1$ and $I(n + 1) = I_2$, whereas for the second one, $I(n) = I_2$, $I(n + 1) = I_3$, and so on.

Quantitative measurements of possible nonlinear determinism, or

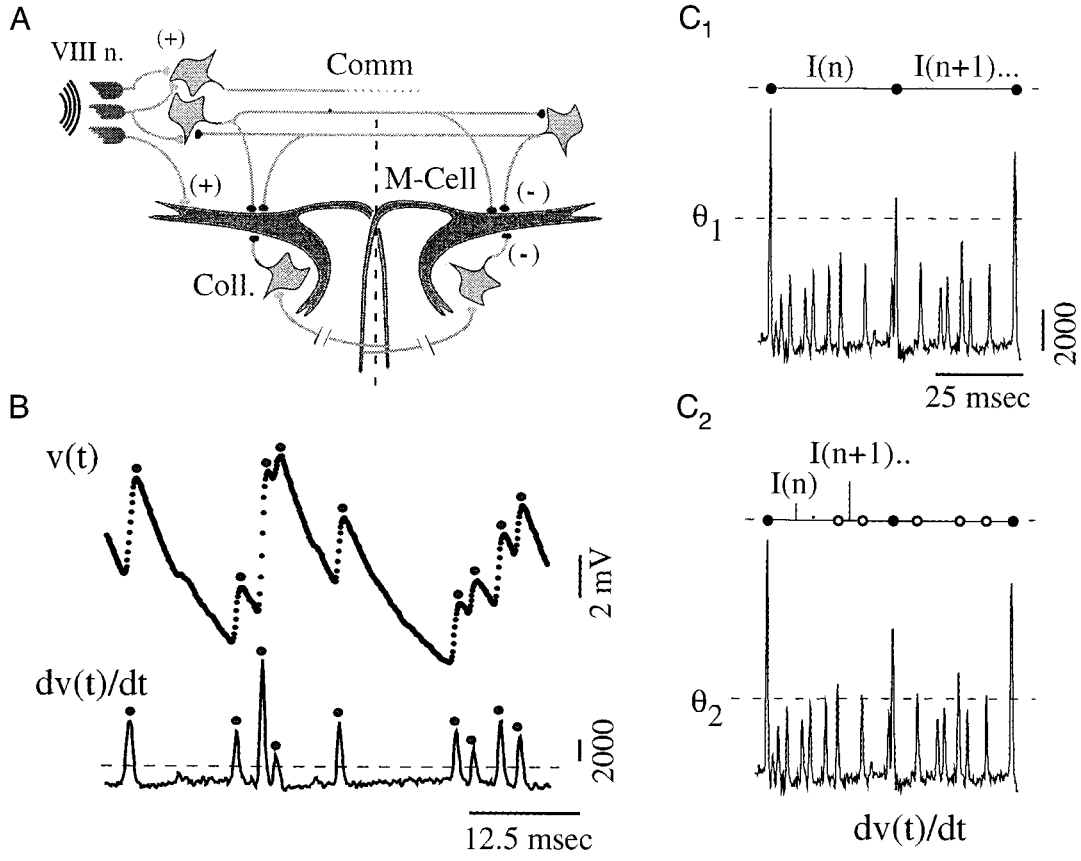

FIG. 1. Experimental network and illustration of the threshold method. *A*: Mauthner (M) cell's inhibitory pathways with commissural interneurons (Comm.) activated via VIII nerve fibers and the recurrent collateral (Coll.) pathway. + and −, excitatory and inhibitory connections, respectively. *B*, *top*: sample of synaptic noise (SN) recorded at a fast sweep speed with consecutive inhibitory postsynaptic potentials (IPSPs) observed as depolarizing events due to the Cl− loading and indicated by dots [$V(t)$]. *Bottom*: corresponding time derivative [$dV(t)/dt$]. Note that the upstroke spikes can be easily distinguished from the background instrumental noise delineated by - - -. *C*, *1* and *2*: derivative of a segment of SN recorded at a slow sweep speed; spike events each corresponding to a differentiated IPSP were selected by a threshold θ (- - -). *C1*: intervals between each detected event (In) and the next one (In +1) were successively measured (●, *top line*) for further analysis. *C2*: as the threshold was lowered, more events were incorporated in the time series (○).

otherwise stated of the degree to which the studied signals can be distinguished from random processes, were made as explained in APPENDIX A.

Modeling

A mathematical representation of the presynaptic networks and their dynamics consisting of four coupled model interneurons was built following Hindmarsh and Rose (1984) and Rose and Hindmarsh (1985). In this physiologically relevant and widely used model (Abarbanel et al. 1996; Hansel and Sompolinsky 1992; Keener and Sneyd 1998), each *neuron* $i = 1, 2, 3, 4$ is characterized by three time-dependent variables: x_i, the membrane potential; y_i, a recovery variable; and z_i, a slow adaptation current. Let

$$\frac{dx_i}{dt} = y_i - x_i^3 + 3x_i^2 - z_i + I_0 + I_i \quad (1)$$

$$\frac{dy_i}{dt} = 1 - 5x_i^2 - y_i \quad (2)$$

$$\frac{dz_i}{dt} = r[S_i(x_i - C_x) - z_i] \quad (3)$$

where I_i is the external current into *cell i*, I_0 is the injected current, C_x the voltage threshold for spike generation, S_i is the scale of the influence of the membrane voltage on the slow dynamics, and r is the time scale of the slow adaptation current. Depending on the values of these parameters, the individual neurons may be in a steady state and generate a periodic low-frequency repetitive firing (LFRF), chaotic bursts, or a high-frequency firing. In our tests, a LFRF was obtained with $I_0 = 3.281$, $r = 0.0021$, $C_x = -1.6$, and S_i was in the range of [2.9–3.3]. For each neuron, S_i was chosen to set fire at one of the frequencies detected by our analysis of experimental data.

Synapses linking neurons were formalized as

$$I_i = -\sum_{j=1}^{N} g_{in}(t - t_j)(x_i - E_{in}) \quad (4)$$

where I_i is the total synaptic input to *neuron i*, N the total number of inhibitory synapses established on their target by the modeled neurons (see diagram of Fig. 7*A*), E_{in} is the reversal potential of the inhibitory current (here set to -3), and t_j is the arrival time of a presynaptic spike. The latter induced a conductance change $g_{in}(t)$ having a time to peak, ttp $= 1$ ms and a decay time, $\tau = 6$ ms, corresponding to physiological values determined experimentally at M cell's inhibitory glycinergic interneurons (Faber and Korn 1978, 1982; Korn and Faber 1976). $g_{in}(t)$ was modeled with an alpha function according to Wilson and Bower (1989). The equations were solved with time steps of 0.001 ms, using a fourth-order Runge Kutta scheme that ensures that all interesting variations in the dynamics are represented (Abarbanel et al. 1996). Solutions were desampled to produce time steps $= 0.05$ ms.

Simulations produced different network behaviors depending on the value of $g_{in} = g_{in}(t = ttp)$. These were synchronized antiphase bursts of action potentials for strong coupling, i.e., $g_{in} \geq 10$, asynchronous and intermittent firing for intermediate coupling $3.5 \leq g_{in} \leq 10$, and continuous firing of the neurons with slight fluctuations around a mean frequency for small coupling values such as $g_{in} \leq 3.5$.

Simulations for this paper corresponded to the third case.

Induction of LTP

LTP of M-cell inhibitory synapses was produced by trains of sounds delivered by a loudspeaker placed in the vicinity of the fish (50 ms, 500 Hz, and 75 dB) repeated every 4 s over 3 min (Oda et al. 1998). As in previous studies (Korn et al. 1992; Oda et al. 1995), the method for assessing the resulting increase of inhibitory synaptic strength was based on measurements of the reduction in the antidromic spike height due to the inhibitory shunt. Since this action potential propagates passively into the soma (Furshpan and Furukawa 1962), any conductance change can be calculated as $r' = (V/V') - 1$, where V and V' are spike amplitudes in the absence and presence of inhibition, respectively. This expression represents the ratio (or fractional conductance) G_{IPSP}/G_m, the two terms being the inhibitory and resting conductances, respectively (Faber and Korn 1982).

RESULTS

In previous studies, we have shown that nonrandom patterns can be observed in SN (Faure and Korn 1997, 1998b), but their detailed organization has not been elucidated despite their striking appearance in the form of well-delineated triangles in PMs. Thus several questions have been addressed in the present study. The first was to identify the classes of dynamical systems and related synaptic events that can produce such geometric figures. The second was to determine what can be inferred about the functional organization of the presynaptic networks that generate the recorded SN. This led us to investigate how the firing patterns of these networks are transferred to postsynaptic cells. The overall conclusion of this investigation is that even though synaptic transmission is probabilistic, SN is a true signal that offers insight on the state of firing of the presynaptic networks.

Periodic components in SN

The recorded signal $V(t)$ showed large oscillations made of successive inverted IPSPs with a magnitude up to several millivolts (Fig. 1*B*, *top*). The time derivative dV/dt of this signal provides an index of the onset and size of each event: the beginning of an IPSP was apparent as a rapid increase in slope reaching a maximum during the rising phase of the synaptic potential (Fig. 1*B*, *bottom*). The size of the resulting spike was proportional to that of its parent IPSP.

Figure 1*C* illustrates the basic method used for this study. Subsets of events were selected, according to their amplitudes, by a threshold θ in such a manner that as this threshold was lowered an increasing number of events was included in the resulting time series. The use of multiple-threshold levels to produce corresponding trains of events derived from the same dV/dt recording (Fig. 2*A*, *1* and *2*) allowed us to take into consideration the information contained in both their timing and relative amplitudes.

For example, the distribution of interspike intervals (ISI) obtained with the events which crossed the highest θ ($=\theta_1$) were multimodal (Fig. 2*B1*). This confirmed their regular periodicity (see also Faure and Korn 1997), which can also be evidenced with autocorrelations (Hatta and Korn 1999). But for lower θ, this periodicity was blurred, and time intervals possessed no obvious structure when the lower-amplitude IPSPs were taken into account (Fig. 2*B*, *2* and *3*).

Power spectra of the spike point process showed additional organization of the trains. In the illustrated case, even at θ_3 (Fig. 2*C*), there was a broad peak between 60 and 80 Hz. This result was interesting but difficult to interpret. The simplest explanation, that the events were approximately periodic with a period of roughly 12–16 ms, was clearly ruled out by the ISI histogram (Fig. 2*B3*), which shows that interspike intervals

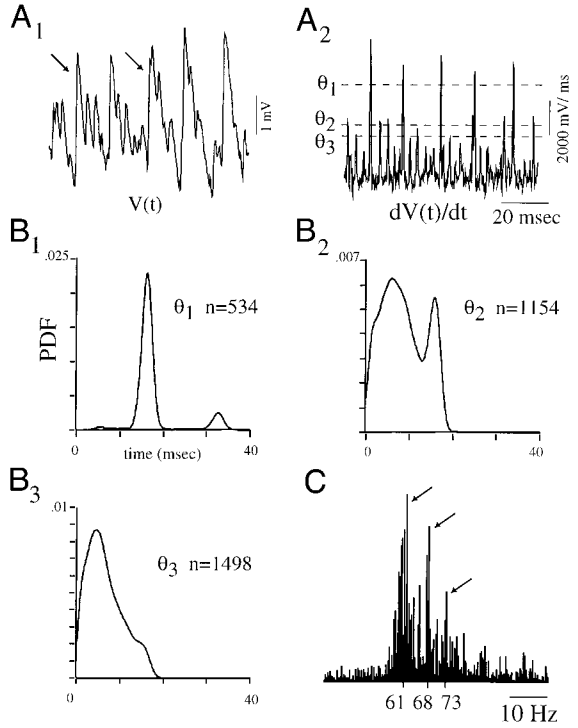

FIG. 2. Classical 1st- and 2nd-order analysis of SN. *A1*: inhibitory SN with inverted IPSPs, 2 of which are indicated by →. *A2*: time derivative of this signal with different levels of thresholds ($\theta_1 - \theta_3$) used to select progressively smaller events. *B, 1–3*: probability density functions (PDF) of time interval histograms from a 10-s segment of recording. *B1*: at threshold θ_1, a dominant periodicity of 16.4 ms is revealed. *B, 2* and *3*: at θ_2, the periodicity tends to disappear (*B2*) and the interevent histogram finally becomes suggestive of a random process (*B3*). *C*: power spectrum of the point process of detected events at θ_3, with a peaky distribution suggesting several superposed time scales (but see text for comments). Some of them (indicated by →) were later identified in the return maps (see Fig. 5, *C* and *D*).

(ISIs) were typically less than 10 ms. Another interpretation, which as shown in the following text is correct, is that this train comprised several interwoven periodic components. Unfortunately, such a structure is difficult to deduce from the power spectrum since there are few objective criteria to count the number of peaks particularly when drifts in frequencies may confound the situation. Furthermore power spectra are insensitive to phase relationships and therefore cannot provide insights into the relationship between oscillators that is typically a nonlinear phenomenon.

In contrast the PMs showed a highly structured pattern. At a high-amplitude threshold, θ_1, the IPSPs were strongly periodic. This appeared (Fig. 3*A1*) as a small circular cloud: each ISI was followed by an interval of approximately the same duration corresponding, in the illustrated experiment, to a principal frequency, fp, the value of which (60 Hz) was the same as that of the main peak in the ISI histogram of Fig. 2*B, 1* and *2*. At θ_2, more events were included in the PM which showed a triangular (Faure and Korn 1997) or, better stated, a signal-flag pattern. The summit of this motif was centered on fp. This striking figure was observed in 70% (i.e., 21/30) of the experiments where SN could be recorded in stable conditions. At this level there was also an outlined space filled on the lower left triangle (Fig. 3*A2*), and at θ_3 there was only the lower left triangle (Fig. 3*A3*).

A systematic search was carried out to determine if other periodic components were buried in SN. For this purpose, events associated with fp were subtracted from the time series isolated by θ_3 (Fig. 3*B1*), and the maps were reconstructed with the remaining events. This procedure disclosed a distinct second signal-flag pattern, centered on a secondary frequency fs. In this experiment, fs was equal to 68 Hz (Fig. 3*B2*), and overall we found fp < fs in the 12 of 21 experiments where additional triangles could be revealed.

These results suggest that the IPSPs in SN are organized in a primary periodic train of high-amplitude and frequency (fp) and in a second train of somewhat lower amplitude and frequency (fs). As shown in the following text, other intervening and smaller events correspond to at least a third oscillator, (ft).

Interpretation of the PMs

A simple theoretical analysis consistent with experimental data helps to interpret the signal-flag pattern. Consider a sequence of events (Fig. 4*A*) consisting of evenly spaced IPSPs (labeled P) having an amplitude greater than θ_P and period of π_P and another sequence of smaller events (labeled S) having an amplitude near θ_S and period π_S, which are intermingled with the larger P components. The sequences that are used to construct the ISIs depend on the setting of the amplitude threshold. Overall, maps constructed with interwoven periodic S and P events and with some missing S will produce a PM with points scattered on the four lines shown in Fig. 4*B*.

Specifically, when the threshold is between θ_P and θ_S, only the P events will be detected. The resulting sequence can be denoted PsPsPsPs, where capital letters stand for events that are above the threshold. At this level, the sequence of ISIs will be $\pi_P, \pi_P, \pi_P, \ldots$ and the PM will be a single dot at the position marked PsPsP. A small amount of random variations in π_P will broaden this dot into the type of the circular cloud seen experimentally.

At a lower threshold, near θ_S, some S events will be detected and the resulting sequence of events is PSPSPsPS. The ISI comes from consecutive triples, e.g., PSP, SPS, or SPP. Pairs of intervals from PSP triples, e.g., I_1, I_2 and I_3, I_4, in Fig. 4*A* span the period π_P, and they appear in the PM along the diagonal line marked π_P. For SPS triples, the dot can be anywhere in the square bounded by π_P, but when the S-type events are periodic, SPS triples lie on the diagonal line corresponding to π_S. When S events fall below θ_S, triples will be of the form PsPS, SPsP, or PsPsP. These appear on the vertical or horizontal lines of the signal-flag pattern or at their intersection, respectively.

Finally, PMs constructed with thresholds below θ_S also exhibit points in the lower left triangle already evident in Fig. 3*A, 2* and *3*. These points correspond to the events denoted T that were also assumed to be part of a periodic sequence.

A careful examination of the experimental PMs confirmed this interpretation. For example, the principal and secondary periods $\pi_P = 16.25$ ms and $\pi_S = 14.4$ ms detected at the summit of the triangles in Fig. 3, *A2* and *B2*, were also apparent at the border of the highest density areas when the PMs were converted into density maps (Fig. 4*C*). Applying the same protocol to the triangle obtained after excluding P events disclosed a third period $\pi_T = 13.3$ ms at the lower edge of the signal-flag pattern (Fig. 4*D*). The values of these three periods

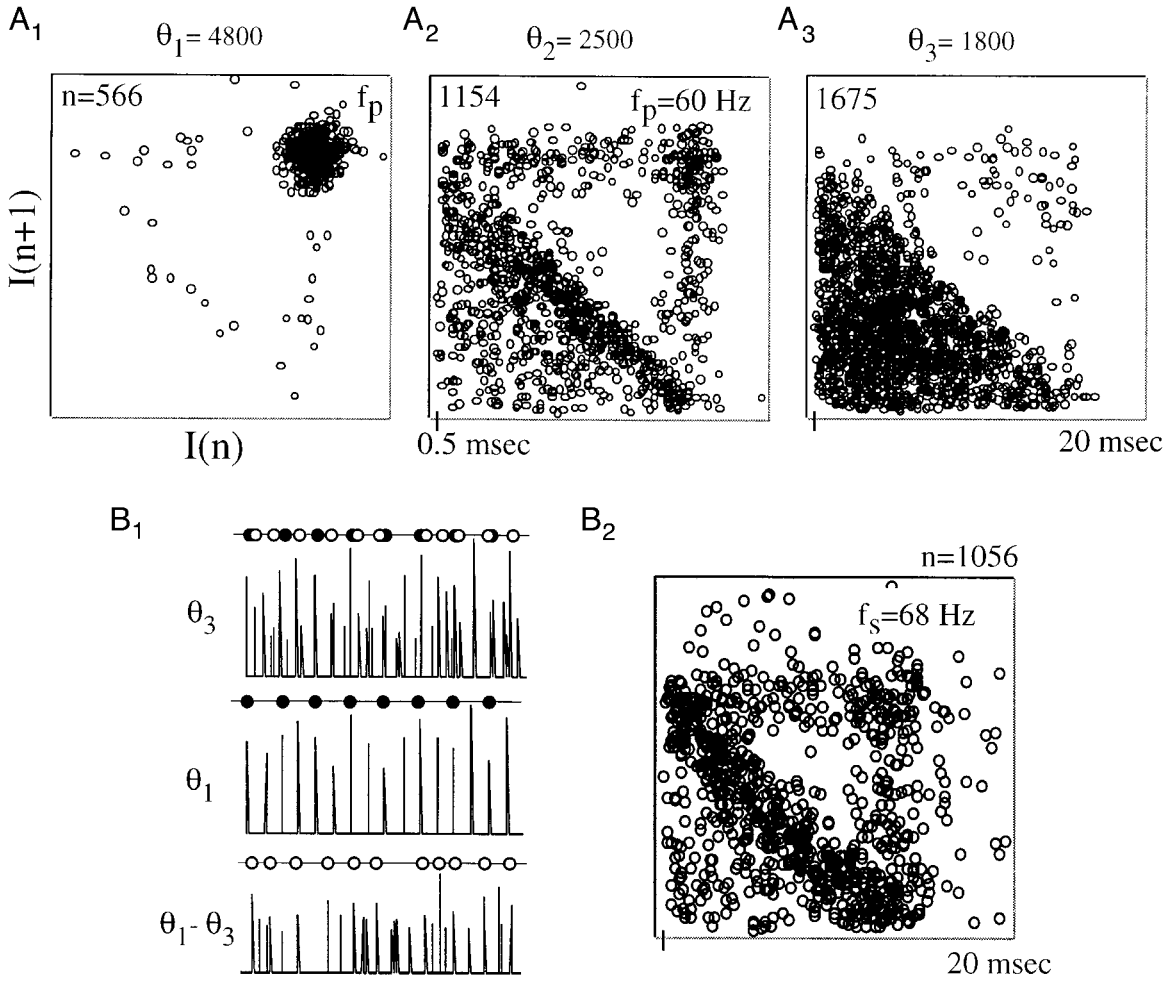

FIG. 3. Analysis of SN with Poincaré maps (PMs). Experimental maps obtained with the 10-s sample of SN (same experiment as in Fig. 2). *A1*: periodic pattern at high-threshold θ_1 with data points centered around a principal frequency (fp) of 60 Hz. *A2*: at θ_2, a signal-flag pattern emerges, with its summit located at fs. *A3*: subsequently this geometric form tends to vanish. Note the lack of interval data less than 0.5 ms, indicating a lockout, i.e., a lower bound of the detection of 2 closely spaced consecutive events (see DISCUSSION). *B, 1* and *2*: extraction of a 2nd periodic component. *B1*: events of the time series showing a sample of the IPSPs selected by θ_3 and used to construct the map of *A3*. Some of these events (●) were already detected at θ_1 (*middle*) but their removal resulted in a new series in which small IPSPs (○) were predominant (*bottom*). *B2*: the return map obtained with this remaining time series disclosed a hidden signal-flag pattern centered on a secondary frequency fs (=68 Hz).

helped to make sense of some of the peaks revealed by the power spectrum of Fig. 2*C* (arrows).

Are the presynaptic oscillators coupled?

The experimental PMs, corroborated by the power spectra, indicated that activities in the presynaptic interneurons that generate SN are rhythmic. However the linear signal-flag structures in the experimental PMs were broader than those expected if the P and S events were exactly periodic (in which case they would lie exactly on the 4 lines of Fig. 4*B*). Two explanations were possible. One was that π_P, π_S, and π_T were independent of each other and varied randomly. The other was that, as in other neuronal systems (Keener and Glass 1984; Pei and Moss 1996), the parent oscillators of the P, S, and T events are coupled to one another, thus producing fluctuations in the periods.

An analysis of the time intervals between the IPSPs comprising SN was carried out to distinguish between three distinct alternative possibilities. First, if the two oscillators P and S are independent, S events will occur with equal probability at any position in PP intervals (Fig. 5*A*, *top*). Second, if the oscillators are phase locked, for example by a strong synaptic path with a fixed delay, PS intervals will remain constant (Fig. 5*A*, *middle*). Finally, in case of a functionally weak synaptic coupling, the oscillators exert complex influences on each other and depending on the previous timing of P and S events, the phase of a subsequent one will be advanced, retarded, or remain the same (Fig. 5*A*, *bottom*).

When PSPSP sequences corresponding to periods π_P and π_S were extracted from SN and ranked as in Fig. 5*B1*, we found that intervals P_1P_2 and S_1S_2 were strongly correlated and that S events were not homogeneously distributed between P ones as would be the case if the oscillators were independent. This phase relationship was quantified, as illustrated by the plot of Fig. 5*B2* (black circles) in which the regression line shows a statistically significant ($P < 0.001$) rejection of the null hypothesis that the SS and PS intervals were independent. Furthermore when the largest, though unclear (due to their timing) S events were incorporated in the analysis (Fig. 5*B2*, blue circles), the slope became even more

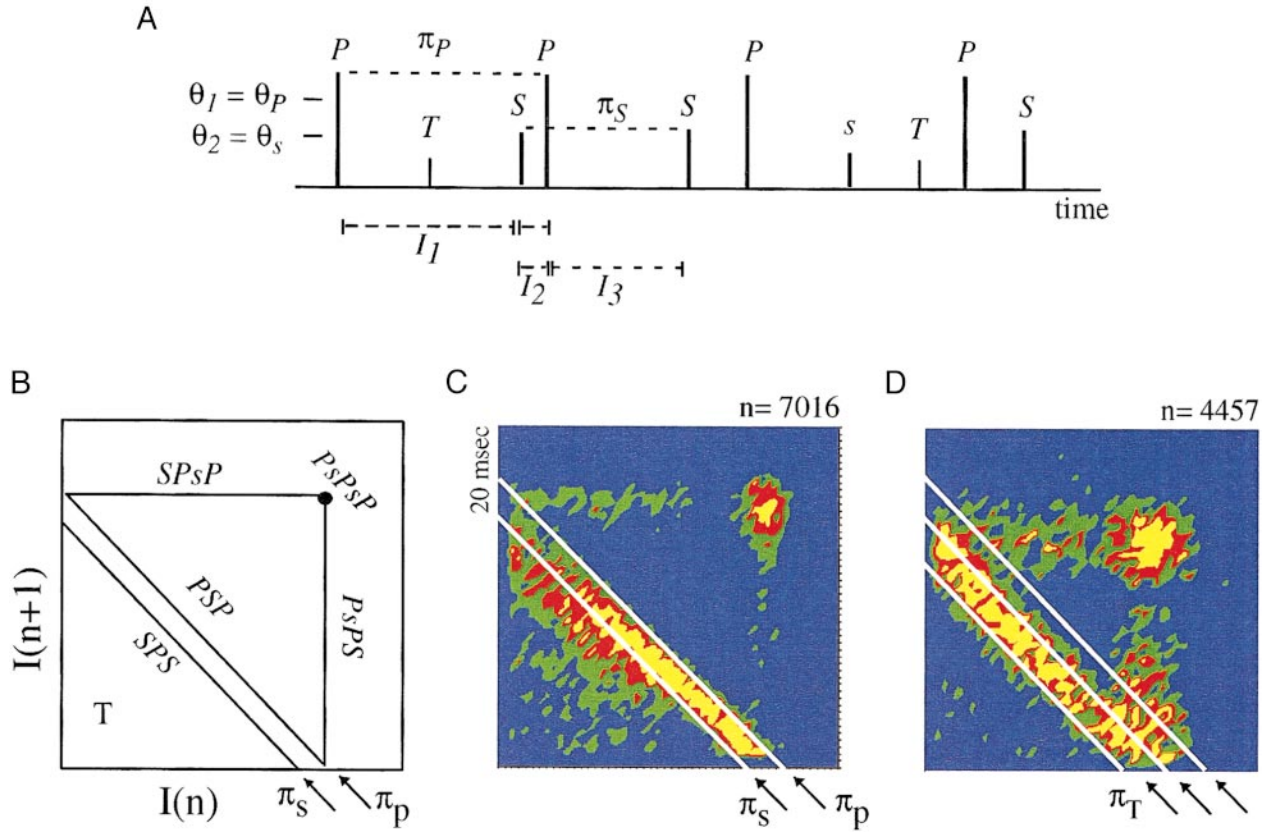

FIG. 4. Construction of the different parts of the signal-flag pattern. *A*: the notation is explained with a schematic d*V*/d*t* time series comprising 3 classes of periodic IPSPs, labeled P, S, and T according to their parent frequency. Events below a given threshold of analysis are in lower case. *B*: interpretation of a theoretical map using the same notation as in *A* to designate the origin of the data points lying along the different arms of the triangle. Lines π_P and π_S mark the diagonals determined by the principal and secondary periods. Points below concern intercalated T's. *C*: evidence that the principal (π_P = 16.25) and secondary (π_S = 14.4) periods fit the highest density of points on a PM constructed with a set of 6 successive time series corresponding to 10 s of recording each (same experimental data as for Fig. 3*A2*). The density was calculated by partitioning the space in 50 × 50 square areas (i.e., with a resolution of 0.42 × 0.42 ms) and by counting the number of points in each of these boxes. Areas in blue, green, red, and yellow indicate regions containing less than 4 points, between 4 and 8, 8 and 12, or more points, respectively. *D*: same protocol as for *C* applied to the experimental data of Fig. 3*B2*. Note that the return map is consistent with the 2-period theory, but shifted: the slow periodicity is now π_S = 14.4 ms and a faster period, π_T = 13.3 ms is unmasked. Here colors pertain to areas containing less than 2, between 2 and 4, 4 and 6, or more points, respectively.

pronounced. Thus the plot of Fig. 5*B2* can be taken as indicating that the S events did not occur during the first 20% of the PP cycle, SS intervals were dramatically prolonged when a S event occurred in the first half of the PP interval, and these intervals were shorter when the S events occurred later in the PP sequence. These three forms of mutual interaction are consistent with a weak coupling between oscillators.

This coupling was not strong enough to phase-lock the S and P events to a stable and constant interval, but it could produce short sequences that exhibited almost constant phase relationships between the P and S oscillators. Advance and retreat patterns (ARPs), similar to those seen previously (Faure and Korn 1997), were observed in the PMs (Fig. 6*A*). These stemmed from the slow drift in phase between S and P events. When the two oscillators were half a cycle out of phase they appeared as a fixed point (Fig. 6*A*, 2) but since they were not phase locked, this point was unstable and the next points labeled 3 and 4 in the PM diverged along a well-defined path resembling that of unstable periodic orbits (UPOs) often associated with chaos (So et al. 1998). Other types of period 1, 2, and 3 orbits were also found (Fig. 6*B*).

These different configurations correspond to the various sequences of time intervals between events outlined in Fig. 6*C*. They stress the diversity of temporal structures contained in SN. The period-1 orbits correspond to a single interval between successive events. Period-2 orbits correspond to two different alternating intervals, while period-3 ones include three distinct sequential repeated intervals and these iterations can be generalized to *n*. The construction of the ARPs is more complex: the successive intervals converge toward and tend to stabilize around a fixed one, but they rapidly escape following distinct paths as illustrated in Fig. 6*A*.

Finally it should be stated that the measures of determinism, i.e., the percentage of determinism (%det) and the $\mu(\epsilon)$ entropy (see details in APPENDIX A), were statistically significant in 19 of the 21 experiments when compared with surrogates, confirming the nonlinear properties of SN.

Complex patterns in presynaptic networks

Numerous reports have demonstrated that coupled neurons can behave as oscillators and generate a vast repertoire of

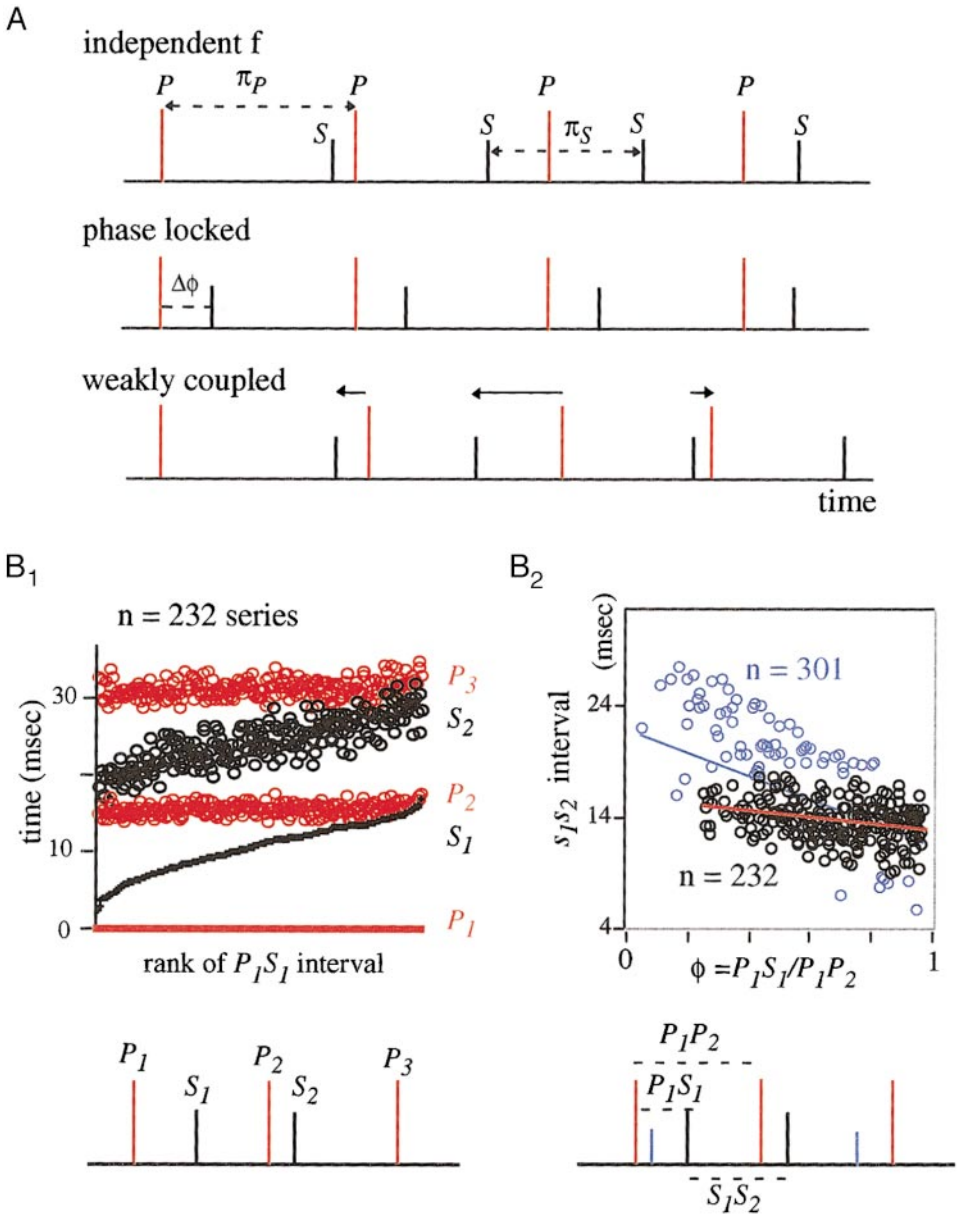

FIG. 5. Interactions between the periodic components. *A*: schemes of the possible timing of P (red) and S (black) events generated by 2 oscillators, depending on their mode of interaction. The S events are located anywhere (*top*) or at fixed distance $\Delta\phi$ (*middle*) in the PP intervals, if the oscillators are independent, or if they are phase locked. In both cases, π_P and π_S intervals are constant. If the oscillators are weakly coupled (*bottom*), they exert more complex effects on each other and successive events, can be advanced or delayed, or remain unaffected in directions indicated by arrows, and π_P and π_S vary (see also text). *B1*: evidence for coupling between periodic IPSPs (same data as for Fig. 3–5). Series of 5 consecutive IPSPs, each corresponding to an unambiguous and almost regular PSPSP sequences are ranked (from *left* to *right*) according to the value of the interval between the first P and S events of the sequence (see the diagram *below*). Note the strong correlation between the P_1S_1 and P_2S_2 intervals. *B2*: ratio of the S_1S_2 intervals as a function of their position in the P_1P_2 intervals, parametrized by the ratio $\phi = P_1S_1/P_1P_2$. Note that larger ϕ are associated with shorter SS intervals [red line $n = 232$ series (black points), slope $= -3$ ms, $P < 0.001$, *t*-test]. If less regular sequences (blue symbols) are incorporated, this relationship becomes even stronger ($n = 301$ series, slope $= -10.8$ ms, $P < 0.001$).

dynamic responses, ranging from periodic to chaotic firing patterns (Abarbanel et al. 1996; Borisyuk et al. 1995; Hansel and Sompolinsky 1992; Rinzel et al. 1998). Since periodic events compatible with the involvement of coupled presynaptic "oscillators" were detected in SN, we assumed that the role of the M cell in the oscillations is simply a read-out function, and we investigated whether coupling between inhibitory interneurons terminating on the M cell can produce complex patterns similar to those observed in actual data. We found that a deterministic model, which does not involve random fluctuations, can reproduce all the major features of the signal-flag geometry, including the broadening of the diagonal PSP and SPS lines of Fig. 4.

Four interneurons were modeled as described in METHODS. They were linked by inhibitory synapses (Fig. 7*A*) generating IPSPs having a fixed latency and a constant amplitude to eliminate all sources of randomness. Values of this model's parameters were set to obtain low-frequency periodic patterns of firing of the same order than those of the different classes of IPSPs revealed in PMs.

Figure 7*B* shows that each of the neurons produced trains of action potentials that were roughly periodic but fluctuated around a given mean period. Such deterministic fluctuations might account for the complexity of the experimental time series (see following text). However, the sum of the impulses produced by the four neurons took the undefined form of a random process and the corresponding return maps (Fig. 7*C*) were similar to those obtained by plotting events selected in actual data by a low threshold, as in Fig. 3*A3*.

Since most highly structured PMs were those constructed with intermediate thresholds θ_2 and suggested the interplay of rhythms from two oscillators, we focused our attention on the behavior of two of the modeled neurons alone. For example, in the case of Fig. 8*A*, the two investigated cells fired with a mean frequency of 57 and 63 Hz, respectively. Yet, the intervals between the action potentials in the summed train were irreg-

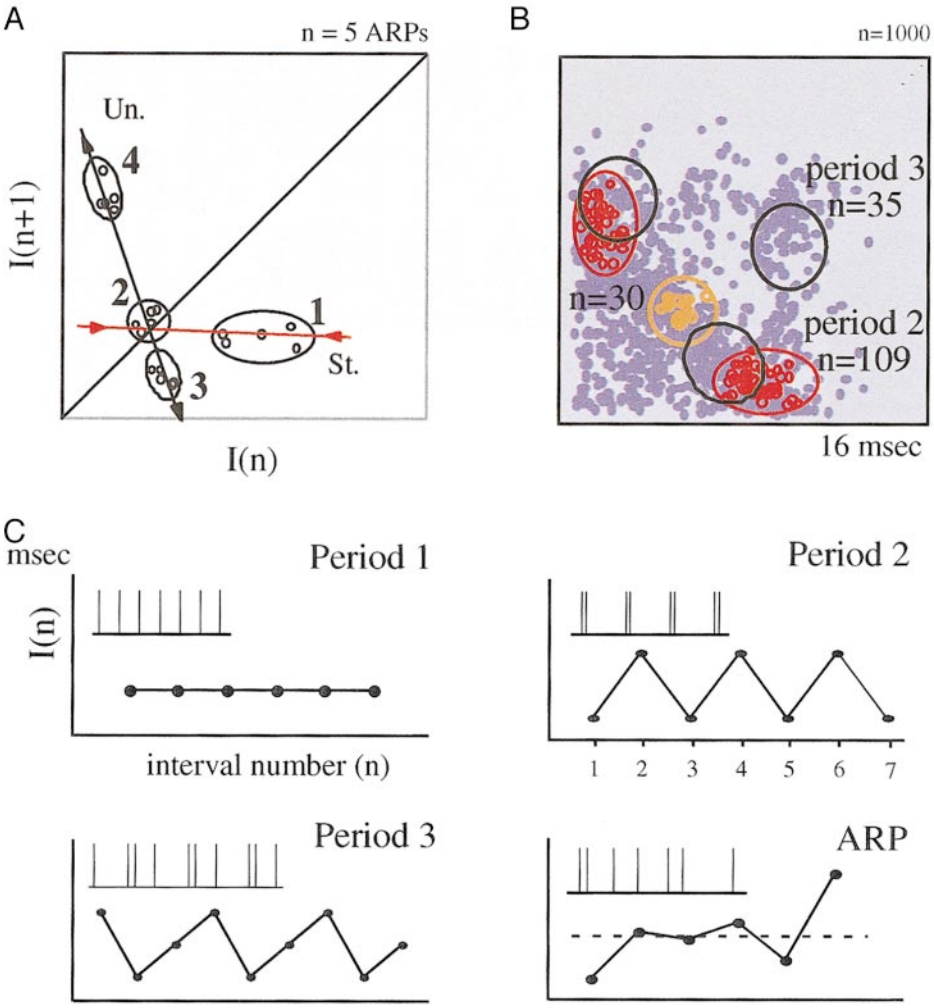

FIG. 6. Further evidence for a weak coupling between the presynaptic oscillators. *A*: advance and retreat patterns (ARPs, $n = 5$) with stable (St) and unstable (Un) manifolds determined by sequences of points that converge toward, and then diverge from, the period-1 orbit (here labeled 2), in the indicated order. *B*: map from the same experiment (shaded). Circles mark multiple occurrences of period-1 orbits (orange, $n = 30$, at least 4 iterates for each occurrence), period-2 and -3 orbits (red, $n = 109$, black, $n = 35$ respectively, at least 6 iterates). *C*: schematic classification of the major patterns found in SN (see text for explanations) that account for the dynamical patterns shown in *A* and *B*. Plots of interval values (ordinates) against interval numbers (abscissa) in the corresponding sequence of events represented by vertical bars (*insets*). Note that in the case of ARPs, the time intervals alternate around a fixed point (dashed line): they first tend to decrease and then to increase sequentially.

ular with phase shifts analogous to those produced by weakly coupled oscillators.

Return maps constructed by plotting these intervals exhibited a well-delineated motif made of series of points distributed around π_P and π_S (Fig. 8*B1*). That is, they were distributed in the same region of the base of the signal-flag pattern obtained experimentally. One can also note in the PM a few distant points (crossed arrow) that mark the intervals between action potentials occurring before and after a pair of synchronous ones (Fig. 8*A*, crossed arrow). They are the precursors of the summit of a complete signal-flag pattern.

The scattering of points around π_P and π_S indicates that the weak coupling between the oscillators produced a deterministic dispersion of the time intervals between events (Fig. 8*B1*), although the simulations did not incorporate external sources of noise. These deterministic fluctuations produced ARPs that resembled those observed in the experimental data (not shown) and period-2 orbits (Fig. 8*B2*).

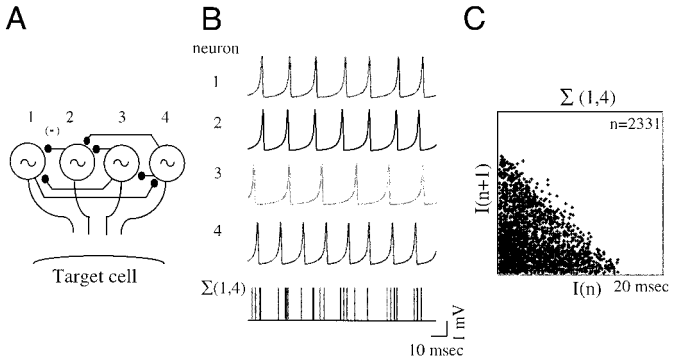

FIG. 7. Model of activity in a presynaptic network of inhibitory cells. *A*: diagram of the formal neurons (labeled 1–4), coupled by inhibitory chemical junctions (−, black dots) and set to fire at 57, 63, 47, and 69 Hz, respectively. *B*: sample of membrane voltage produced by the 4 cells (labeled 1–4), illustrating the resulting spike trains. The summed network output [Σ(1,4)] is shown in the bottom line, with the spikes transformed into upstroke bars of amplitude 1. *C*: return map constructed with the summed series.

Role of synaptic properties in the transmission of presynaptic patterns

The various components of the signal-flag patterns were all evident in the same train because some types of events were sometimes above and sometimes below threshold, the fluctuations of their amplitudes allowing the signal-flags to convey information about the periodicities of each of the oscillators. In addition the distribution of amplitudes allowed for gradual transitions among the types of signal-flag patterns as the detection threshold was lowered with, consequently, a reduction in the number of failures of detection. Therefore by examining the fraction of missed events at each level of θ, we could approximate the extent of the overlap of some IPSPs produced

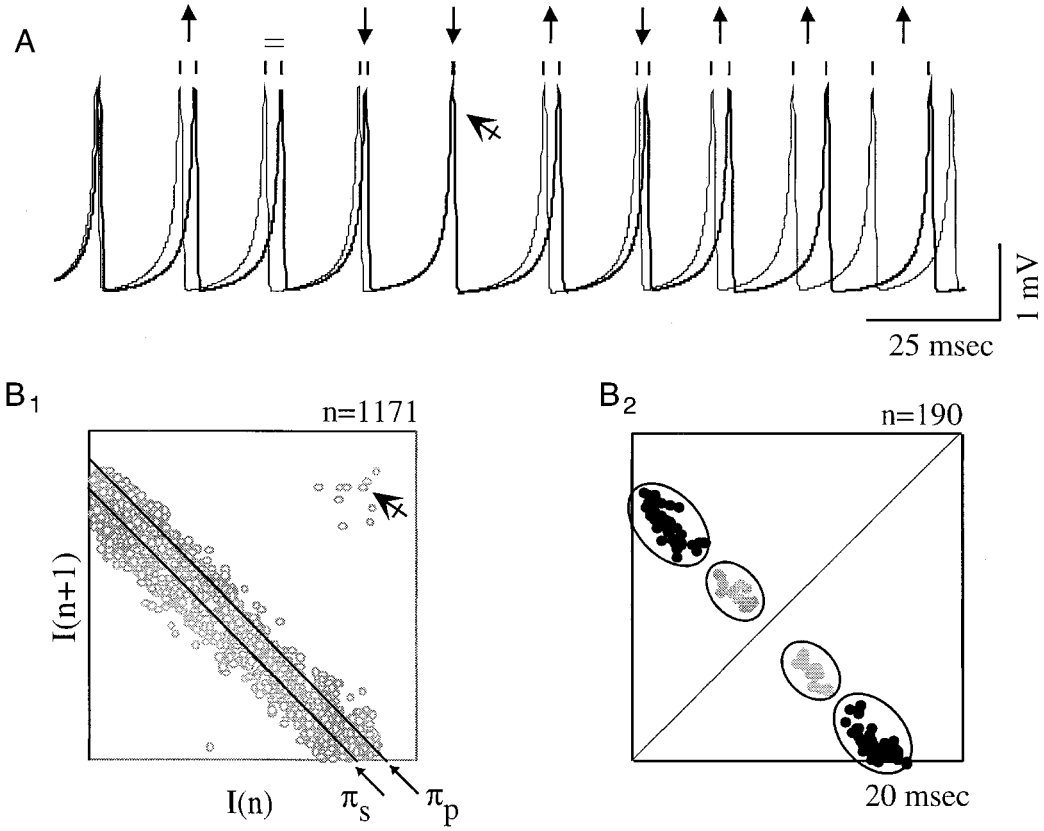

FIG. 8. Deterministic patterns in modeled presynaptic neurons. *A*: trains of action potentials produced by simulated *cells 1* and *2* (thick line) of the network, showing variations of time intervals resulting from weak coupling between these neurons. Symbols above spikes correspond to changes in their relative timing. The intervals between spikes of the 2 cells can increase (up arrow), decrease (down arrow) or remain unchanged (equal sign) when compared with the preceding 1. The crossed arrow indicates synchronous spikes. *B1*: return map (shaded) constructed with the intervals between all presynaptic "action potentials" produced by *cells 1* and *2*. Note the broadband around the diagonal lines $\pi_P = 17.5$ and $\pi_S = 15.8$ ms, arising from the purely deterministic coupling of the involved oscillators. *B2*: multiple occurrences of period-2 orbits in the 2 regions (black and gray dots) delineated by circles.

by each oscillators (APPENDIX B1). The amplitude fluctuations of these IPSPs were consistent with an involvement of synaptic junctions. We found that indeed, connecting the formal interneurons with terminal synapses that "released" transmitter in quanta according to principles established at chemical junctions allowed the model to reproduce the hierarchical features of the PMs.

Chemical transmission is governed by two parameters, *n* and *p*, where n represents the population of basic "quantal units" *q* capable of responding to a nerve impulse, and *p* their average response probability (Del Castillo and Katz 1952). Then the product *np* is the so-called mean quantal content, which is equal to the average number of quanta released by a given junction during successive trials, while the product *npq*, where *q* is the size of a quantum (set to 1 in our simulations), determines the synaptic strength. Since at central synapses transmitter release can follow a simple or a compound binomial statistics, where *p* is the same or is different for every site of release established by a neuron on its target (for a review, see Korn and Faber 1991; Redman 1990), we tested these two models in this study.

First, a simple binomial model, previously shown to account for the amplitude fluctuations of IPSPs evoked in the M cell by its presynaptic interneurons (Korn et al. 1982), was used with values for the terms *n* and *p* in the range of those derived in earlier experiments (Korn et al. 1986).

When the neurons had the same quantal content *np*, all IPSPs fluctuated in the same range (Fig. 9*A*, *1* and *2*) and the signal-flag pattern did not appear in the PM (Fig. 9*A3*). This result was easily explained by the fact that any threshold detected the same proportion of IPSPs regardless of their parent cell and despite small changes at the extremities of the inverse cumulative densities of the amplitude events (Fig. 9*A2*, ↓). These slight discrepancies were due to small differences in the coefficient of variation (CV) of the amplitude distributions of the IPSPs produced by each cell. Similar conclusions were reached with other runs, whatever the values attributed to *n* and *p* of each interneuron, as long as the four modeled cells had an identical quantal content (a justification of this rule, which also pertains for compound binomial statistics, can be found in APPENDIX B2).

When the model was modified to include different *np* products that distinguish presynaptic neurons from each other (Korn et al. 1986), the signal-flag pattern was restored in the maps and the ARPs reappeared, as well as period-2 orbits (not shown). This result is illustrated in Fig. 9*B*, *1–3*, for which the "neurons" had a quantal content of 13.3, 6.2, 3.7, and 1.86, respectively. Again, this result can be easily explained. As

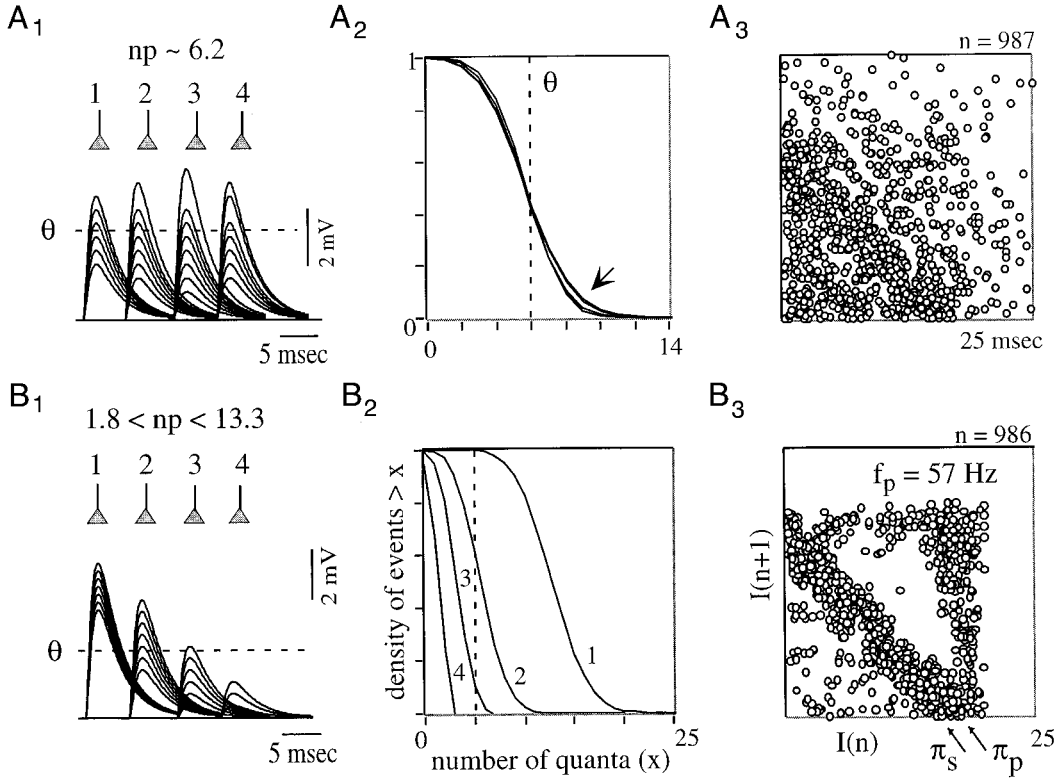

FIG. 9. Contribution of synaptic properties to the transmission of presynaptic patterns. *A, 1–3*: analysis of postsynaptic signals produced by uniform junctions. *A1, top*: same model and parameters as for Fig. 8 but implemented with synaptic terminals labeled 1–4, having different release parameters, i.e., $n = 12$, 14, 20, and 25 and $p = 0.52$, 0.44, 0.31, and 0.25, respectively, and the same quantal content, *np*. *Bottom*: superimposed fluctuating IPSPs ($n = 10$) of statistically equal random sizes generated by each of the neurons. Note that these IPSPs are equally detected by any θ. *A2*: inverse cumulative event density, i.e., density of events with amplitudes greater than a given size expressed in number of quanta (x, ordinates) or otherwise stated, percentage of detected events, as a function of the number of available quanta (abscissa). The 4 curves are almost similar (except at their extremities—↓—see text). *A3*: the interevent intervals appear as random in the PM. *B, 1–3*: same presentation as in the preceding text but with terminal synapses having different release parameters, i.e., from *left* to *right*, $n = 38$, 20, 8, and 3 and $p = 0.35$, 0.31, 0.47, and 0.62, respectively, and distinct quantal contents. Thus θ detects preferentially IPSPs from oscillators 1 and 2 and the corresponding PM exhibits a signal-flag pattern centered on the frequency of the largest events (fp).

shown by Fig. 9*B, 1* and *2*, at intermediate values, θ identified preferentially IPSPs produced by the first two cells. For example, when θ was set to select the same proportion of events (i.e., ≃42%) as in Fig. 9*A2*, 100% of events from *cell 1* and 60% from *cell 2* were suprathreshold, against only 10 and 0% from *cells 3* and *4*.

Second, the model was implemented with terminals "releasing" according to nonuniform p's. As illustrated in Fig. 10, the results were almost indistinguishable from those described in the preceding text. That is, a signal-flag pattern, ARPs and period-2 orbits became only apparent in PMs when the *np* products were different. This finding was not surprising since the distribution histograms of IPSPs modeled by a compound binomial are roughly similar to those from a simple binomial distribution but with a smaller CV than with a simple binomial statistics.

Finally it should be noted that in these simulations values of n and p were inversely correlated as experimentally observed at M cell's inhibitory connections (Korn et al. 1986). However, this need not be the case (see APPENDIX B2).

Experimental validation

To verify the involvement of synaptic efficacies, we conducted a series of experiments, taking advantage that the strength of the M cell's inhibitory synapses are modified in vivo by LTP, a classical paradigm of learning that can be induced in teleosts by trains of sounds emitted in the vicinity of the fish. This form of LTP is due to an increase of the presynaptic parameter of release p, while n and q remain unaffected (Oda et al. 1995). As in previous reports, the potentiation of the inhibitory synapses was quantified using a parameter r', or fractional conductance, which defines the degree of the inhibitory shunt (see METHODS).

As expected the amplitude of IPSPs comprising SN was increased during LTP (Fig. 11, *A1* and *B1*). Furthermore return maps constructed with a high-threshold (θ_2) were markedly different before and after the conditioning sound trains (Fig. 11, *A2* and *B2*). That is, LTP strengthened the two-oscillator triangular pattern in the PM, as further evidenced by comparing the PMs constructed with a lower threshold, θ'_2 (Fig. 11, *B2* and *C*) and by the 8% increase of the %det (Fig. 11*D*). On the other hand π_p and π_s remained the same (Fig. 12), suggesting a stability of the dynamics in the network.

In four experiments, r' was increased by 29 ± 8.1% (mean ± SE) after the learning protocol, indicating LTP of the commissural synapses (Korn et al. 1992), and the %det was enhanced by 14.3 ± 2.1%. Adding three other experiments,

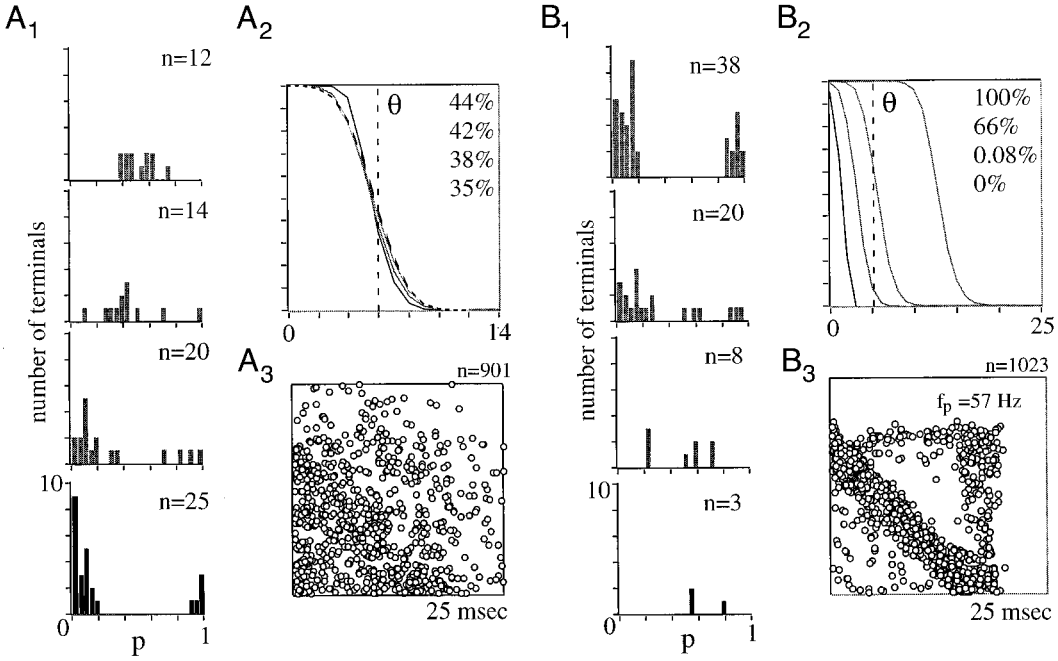

FIG. 10. Analysis of IPSPs produced by nonuniform junctions. Same g as for Fig. 9 but with different probability of release at each terminal (n) of simulated neurons. *A, 1–3*: all neurons have the same quantal content. *A1*: histograms of p values (abscissa) in the terminals of *neurons 1–4* (from *top* to *bottom*) with indicated (n). Mean p values were 0.52, 0.44, 0.31, and 0.25, with a variance of 0.32, 0.45, 0.55, and 0.6, respectively. *A2*: inverse cumulative density of events and threshold θ with indicated proportion of the detected events (same comments as for Fig. 9*A2*). *A3*: corresponding PM with random distribution of interevent intervals. *B, 1–3*: same presentation as for *A, 1–3*, but with terminals having different quantal contents. The mean p were 0.35, 0.31, 0.47, and 0.62, and the variances were 0.63, 0.56, 0.45, and 0.32, respectively. Note the signal-flag pattern in the PM.

during which LTP was only assessed by comparing the amplitude of IPSPs (to avoid further modifications of SN by control sounds), this value became 11.3 ± 1.8%. In another cell, the sounds produced no LTP and the determinism was unchanged.

DISCUSSION

Taken together these results suggest that the information contained in SN permits the dynamics of the presynaptic networks to be reconstructed. This information is contained both in the intervals between IPSPs and in their amplitudes.

Our data can be generalized as follows. Several combinations of P and S events in triplets, some of which result from failures to detect events, are necessary to construct a complete signal-flag pattern. This prerequisite is guaranteed by the "separating power" of the largest np products at the terminals of neurons that generate the SN. On the other hand identified dynamical sequences (ARPs, period-n orbits and other signs of determinism) are found at the base of the signal-flag pattern, and the clarity with which they appear is related to the emergence of both P and S events in the time series. This second condition evidently imposes an irreducible separation between the np products (see APPENDIX B2) that allows the presynaptic dynamics to become predominant in the SN.

Validity of the coupling hypothesis

Two important issues had to be considered before accepting that the coupling between presynaptic interneurons accounts for the patterns observed in SN.

First, might we have incorrectly classified as P, S, or T activities? Our methodology for displaying the coupling between the P and S oscillators relies on the detection of events and their classification as P, S, and T. Thus any failure of detection or classification that is related to the timing of the spikes could artifactually influence the display of coupling. However, when constructing Fig. 5*B2*, we remained conservative and considered only events (shown in black) belonging to unambiguous PSPS quartets. P, S, and T events were selected using a criterion that combines amplitude with timing information. Specifically, P events were obvious and, despite possible confusions between S and T events due to overlap of their size, most S ones could be identified as such in Poincaré maps since they appeared on the diagonal line corresponding to the S period. Second, how reliably could we detect closely spaced events? Events closer than a given time separation were not distinguished in the time series. This issue was important because a sufficiently long lockout can produce the illusion of coupling. But this lockout was approximately 0.5 ms, and there are few points with short ϕ in Fig. 5*B2* simply because there were few PSPS quartets. Theoretical analysis shows that the 0.5 ms lockout is too short to produce artifacts mimicking the pattern in Fig. 5*B2*. In confirmation, simulations with uncoupled S and P oscillators show virtually no coupling even with lockouts as large as 3.5 ms.

Two additional arguments reinforced the hypothesis of coupling. Data points in the PMs were not uniformly distributed as they would be if the variability of each frequency was random and, as demonstrated by combined electrophysiological and histological studies (Korn et al. 1990; Triller and Korn 1981), commissural inhibitory interneurons presynaptic to the M cell are linked by chemical inhibitory synapses.

Other simulations can produce triangular maps. Such is the

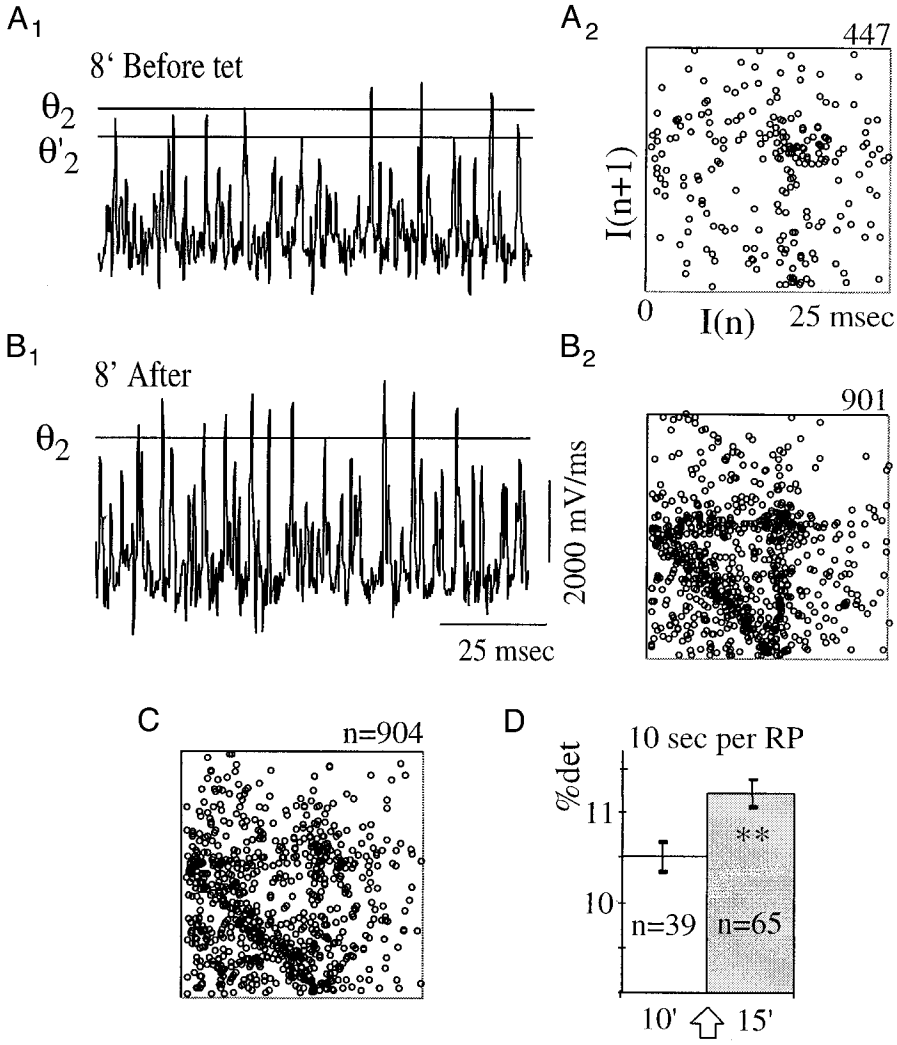

FIG. 11. Changes of temporal patterns during long-term tetanic potentiation (LTP). *A1*: time derivative of a segment of SN recorded 8 min before the conditioning sounds (see text). *A2*: PM obtained with a high-threshold θ_2, showing an emerging cloud around 68 Hz (suggesting a π_P of 14.7 ms). *B*, *1* and *2*: same presentation of SN collected 8 min after the onset of the learning protocol with an increased number of suprathreshold events and a triangular map. *C*: lowering the threshold in *A1* from θ_2 to θ'_2, to match the number of events in *B2*, the map still shows a somewhat different signal-flag pattern. *D*: pooled values of the percentage of determinism (%det) calculated on *n* windows of 10 s each, obtained during the 10 min preceding and the 15 min following the onset (arrow) of the conditioning sound trains (vertical bars are SE). *t*-test significant (asterisks) at 1%.

case for models based on one oscillator producing large events intercalated with smaller ones occurring at random (not shown) or on several independent and noisy oscillators, each making events of different amplitudes, and a fixed level of detection. However when examined in detail, such maps do not exhibit the fine temporal structure (periodic orbits, phase relationships) found in the SN recorded from the M cell.

Finally could nonlinearity in synaptic transmission and/or the responsiveness of the M cell to its inputs create the observed patterns? While this is conceivable, the most obvious sources of nonlinearity so far identified in the M cell system are unlikely to be involved. In particular the effects of presynaptic depression that reduces IPSP amplitudes at high rates of presynaptic firing are stabilized at frequencies more than 33 Hz (Korn et al. 1984). In confirmation no correlation was found between the amplitudes of the successive P events or between their amplitudes and timing. At the postsynaptic level, we investigated whether the nonlinear summation of potential change (Martin 1955) and, more importantly, the voltage dependence of the decay of IPSPs (Faber and Korn 1987) did affect the size of overlapping events. Such seemed not the case since the amplitude distribution of S events was the same during the first half of the PP cycle (which includes the falling phase of the P events) and during the second one.

Neuronal correlates of the presynaptic oscillators

Nonlinear deterministic components have been identified in SN (Faure and Korn 1997, 1998b), and it is well established that coupled oscillators can generate similar patterns, including chaotic ones (Glass and Mackey 1988). The frequencies of the oscillators unmasked in this study are consistent with those of the periodic components already noted in the M cell's inhibitory SN (Faure and Korn 1997; Hatta and Korn 1999), which were in the range of the so-called gamma rhythm observed in higher vertebrates (Jefferys et al. 1996; Singer 1993).

Anatomical and physiological studies have shown that there are more than four interneurons in the M-cell presynaptic network with the estimates being in the range of at least 50 (Faber and Korn 1978; Korn and Faber 1990). Thus it is surprising that the contribution of a few oscillators can be distinguished or, in other terms, that the amplitude of the IPSPs produced by each of these oscillators seems to be ordered according to their origin. Calculations of the average size of the P and S IPSPs may help to address this issue. In the goldfish M-cell system, the size of an inhibitory

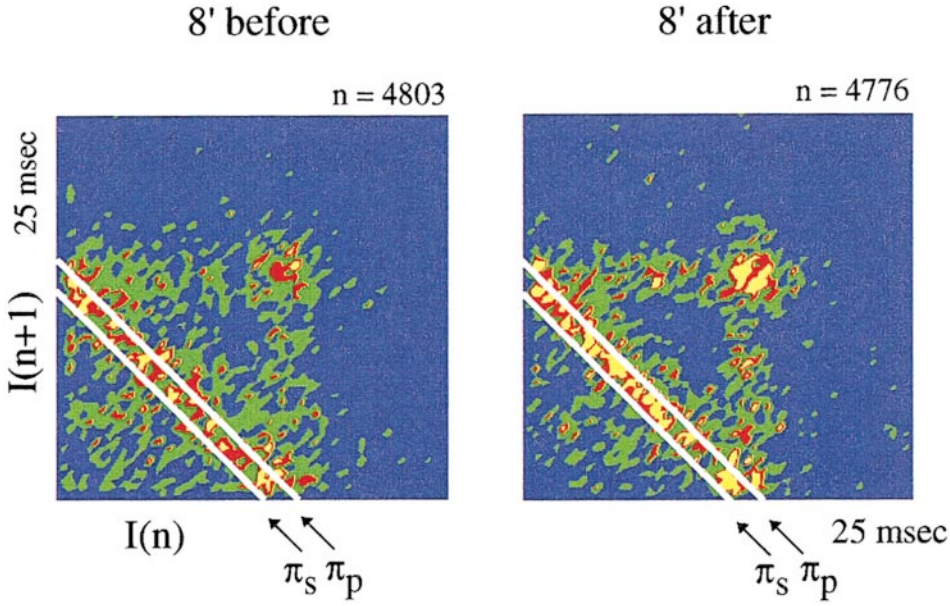

FIG. 12. Stability of presynaptic frequencies after induction of LTP. The principal (π_P = 14.7 ms) and secondary (π_S = 13.3 ms) periods which fit the highest density of points were determined, with the method described in the legend of Fig. 4. Areas in blue, green, red, and yellow indicate regions containing less than 2, between 2 and 4, 4 and 6, or more points, respectively. Here PMs were constructed with sets of five successive time series of 10 s of SN each. Note that π_P and π_S were unchanged after LTP (same experiment as in Fig. 11).

quantum is approximately 1% that of the full-sized collateral IPSP evoked by antidromic activation of the Mauthner cell axon (Korn et al. 1982). The mean unitary IPSPs produced by stimulations at 1 Hz of a single presynaptic interneuron comprise 5.8 quanta (Korn et al. 1986). Furthermore their amplitudes decrease in a known way at increased stimulating frequencies due to presynaptic depression (Korn et al. 1984). Based on these values, estimations made in time series from three goldfish indicated that the P and S IPSPs were, respectively, six to seven and four to five times bigger than the average unitary response.

Several hypotheses that have not been tested in this study might explain this amplitude distribution. One is that these IPSPs are produced by the firing of a special set of cells, that of the rather exceptional "superinterneurons," which evoke IPSPs of unusually high amplitudes (Korn et al. 1986). The other is that a number of presynaptic cells might fire simultaneously. Two signaling mechanisms already demonstrated in the organization of the M cell's inhibitory network could be involved: one is the chemical coupling between inhibitory interneurons that has been shown to underlie synchronization in theoretical models (Jefferys et al. 1996; Traub et al. 1996; White et al. 1998; Whittington et al. 1995) and in experimental material (Bragin et al. 1995; Whittington et al. 1995). The second is that the somata of the commissural interneurons are linked in teleosts via gap junctions (Korn et al. 1977), which favor their simultaneous discharge including those of functionally related inhibitory cells (Gibson et al. 1999).

Arguments offered in APPENDIX B3 indicate that our results do not depend on whether the quanta are issued by synchronously firing cells or are all from a single presynaptic neuron.

Synaptic properties and the transmission of deterministic patterns

Analysis of the PMs indicated that the signal-flag patterns were clearly delineated with maximum values of the measures of determinism [%det and $\mu(\epsilon)$] and the largest number of ARPs, when 99.3 ± 0.32% (n = 10), 49.7 ± 2.57% (n = 10), and 12.1 ± 1.89% (n = 10) of P, S, and T events were included in the maps, respectively. These values agree closely with those of the *np* products required for the construction of "meaningful" maps with models.

We observed in experimental data that the same sequence of event intervals can produce qualitatively different patterns depending on the level of the threshold used to window the sequence. Indeed, the probabilistic nature of transmitter release means that there is a graduated transition between the different patterns as θ is varied. The notion that the probabilistic component p is critical here was confirmed by simulations in which the oscillators had different n's but with $p = 1$ at all terminals, reducing the variance to $\sigma^2 = 0$. This resulted for any level of θ in maps lacking signal-flag patterns. The nonzero variance that results from $0 < p < 0.1$ guarantees that multiple components of the patterns shown in Fig. 4*B* can be present in the signal flags. The value of p sets the relative mixture of these patterns. Changing p, as in LTP, modifies this mixture.

In this context, the probabilistic aspect of neurotransmission, whose function in neuronal communication has not been clarified, becomes an advantage rather than a limiting factor (Zador 1998) since it allows synaptic strengths to be adjusted in a manner that shapes the transmitted information without needing to modify the dynamics of the presynaptic network.

The emergence of the deterministic structures in the postsynaptic cell with multiple inputs is made possible by the nonuniform values of synaptic weights and the stochastic release of quanta. Furthermore the transmission of qualitatively different patterns in the M cell may allow encoding of a small repertoire of motor reactions as suggested by the results of LTP which is known to underlie modifications of the goldfish escape behavior (Oda et al. 1998).

APPENDIX A

A deterministic system is one whose complete behavior can be expressed with an infinite precision in a mathematical description (usually a differential equation). Then if the initial values of all

variables are known completely, the system's entire future history is predictable and can be calculated exactly.

A chaotic system, which often appears at first sight to be random, is also deterministic, but it displays what is called sensitive dependence to initial conditions. That is, solutions obtained with two different starting points can be profoundly different: if the initial conditions are infinitesimally displaced from each other, then the solutions diverge exponentially. The extent to which they are unpredictable depends on this rate of divergence.

The dynamics of deterministic systems are different in principle from random processes where prediction is impossible except statistically.

While the presence or absence of a specific form of determinism was not the focus of this report (for this aspect of the work, see Faure and Korn 1997, 1998b), that of SN was quantified for two reasons. The first was to confirm that SN could be distinguished from a random process. The second was to estimate the modifications produced by external sensory stimuli. Two parameters were used. Both detect so-called recurrent patterns, i.e., sequences which approximatively repeat themselves over time (hidden rhythms). They can be computed in recurrent plots (Eckmann et al. 1987), which are particularly well suited for studies of biological processes.

Let $x(i)$ be the ith point on the orbit describing a dynamical system in a d-dimensional space, for $i = 1, \ldots, N$. The recurrence plot (RP) is an array of dots in a $N \times N$ square, where a recurrent point is placed at the (i, j) coordinates whenever the embedded vectors (xi, xj), defined here by $xi = [I(i), I(i + 1)]$ are within a predetermined cutoff distance (ϵ). The organization of recurrent points into diagonal line segments of length L indicates the parts of the trajectories which are close (under resolution ϵ) during L successive time steps.

The first parameter was the percentage of determinism (%det) (Weber and Zbilut 1994), which is the number of dots included in diagonal line segments divided by the total number of dots in the RP. The second parameter was the slope, $\mu(\epsilon)$, of the exponential decay of the histogram of the number of segments of length L. As demonstrated elsewhere (Faure and Korn 1998b), at limits, this slope is an estimation of the Kolmogorov-Sinai entropy.

To confirm the nonlinear properties of the PMs, we constructed surrogate data. A surrogate is an artificial set constructed from the original data with constrained statistical properties that depend on the null hypothesis being tested. The statistical significance of the two parameters was examined with the null hypothesis that all forms of determinism found in SN were brought about by the linear properties (amplitude and frequency distributions) of the signal. For this purpose, surrogates of the time derivative of the membrane potential and of the raw spike trains, which matched both the amplitudes of the signals and their power spectrum, were constructed using two distinct methods despite their possible limitations when applied to time interval series (Schreiber and Schmitz 2000). These were the amplitude-adjusted method (Rapp et al. 1993; Theiler et al. 1992) and the iterative surrogate technique (Schreiber and Schmitz 1996), which involves an iterative refinement of the latter.

APPENDIX B

This appendix is concerned with the synaptic properties that can lead to the the signal-flag patterns. We treat the amplitude of each event (i.e., of an IPSP in SN) as random and seek to characterize the amplitude distributions of the P, S, and T events.

Appendix B1: percentages of detection

We need some statement about amplitude distributions of each class of IPSPs to express their degree of overlap. Since the release mechanism may obey simple or compound binomial or possibly other statistics (if the quanta are not released independently), we represent the probability distribution of the event amplitudes as a gaussian distribution described by a mean amplitude m and a variance σ^2. We denote the mean amplitude of the different types of events as m_P, m_S, m_T and their variances by $\sigma_P^2, \sigma_S^2, \sigma_T^2$.

As is conventional for a gaussian distribution, any percentile can be depicted in terms of the standardized z measure. For example the 2.5th percentile of a normal distribution lies at $m + z_{0.025}\sigma$. As is found in standard tables of the Gaussian distribution, $z_{0.025} = -1.96$.

The PMs give information about the fraction of events of each type larger than a selected θ, that is, about the percentiles of the distribution. So, the number of missed P's could be assessed in Fig. 3*A1* by computing that of the overlong intervals (with I_n or $I_{n+1} \gg \pi_P$), which do not appear on the PMs due to the chosen scales. Since π_P was known, one could interpolate the position of the missing P's. This procedure indicated 52 of them inferred among the 566, i.e., 92%, detected ones.

Generally in our experiments, there was a threshold at which 95% of P and no more than 5% of T events were detected. This observation can be translated into the z notation as: $m_P + z_{0.05}\sigma_P > \theta$ and $m_T + z_{0.95}\sigma_T < \theta$ (where $z_{0.05}$ is negative). Combining the two statements we have

$$m_P + z_{0.05}\sigma_P > m_T + z_{0.95}\sigma_T \tag{B1}$$

where $z_{0.05} \approx -1.6$ and $z_{0.95} \approx 1.6$.

Similar relationships can be found by comparing other classes of events: the fact that approximately 50% of S and 2% of T are greater than $\theta = 3{,}500$ for the data of Fig. 3 indicates that $m_S + z_{0.50}\sigma_S > m_T + z_{0.98}\sigma_T$ or, substituting in the tabulated values for $z_{0.50}$ and $z_{0.98}$, $m_S > m_T + 2\sigma_T$.

Appendix B2: implications of np values on the percentage of detection

m and σ^2 can be related to the release parameters n and p. For each type of events and assuming binomial statistics, we have $m = np$ and $\sigma = \sqrt{np(1 - p)}$.

Relationships of the form of *Eq.* B*1* can be used to determine theoretical limits on the number of quanta potentially involved in each type of events. For any nonzero value of σ_P and σ_T, this equation directly implies that $m_P > m_T$ and therefore that $n_P p_P > n_T p_T$. In other words, there can be no signal-flag pattern if the np products are equal. This rule can be generalized to a compound binomial. If the n quanta are released with different probabilities, then $m_P = \sum_{k=1}^{n_P} p_{k,P}$, $m_T = \sum_{k=1}^{n_T} p_{k,T}$, $\sigma_P = \sqrt{\sum_{k=1}^{n_P} p_{k,P}(1 - p_{k,P})}$, and $\sigma_T = \sqrt{\sum_{k=1}^{n_T} p_{k,T}(1 - p_{k,T})}$. Then it is easily shown that for fixed n and m the compound binomial has always a smaller σ than the simple binomial distribution.

For both binomial-type models, the smaller are the values σ_P and σ_T, the closer can be m_P and m_T. In the theoretical limits where $\sigma_P = 0$ and $\sigma_T = 0$, it is required from *Eq. B1* that $n_P > n_T$.

Using the coefficient of variation $CV = \sigma/m$, we have from *Eq.* B*1* the relation

$$m_P > m_T \frac{1 + z_{0.95}CV_T}{1 + z_{0.05}CV_P} \tag{B2}$$

where CV_P and CV_T are the coefficients of variation of the P and T events respectively. For example, taking $CV_P = 0.28$ which is the mode of pooled experimental data from M cell's inhibitory connections (Korn et al. 1986), and assuming a similar CV for the S and T events, indicates that $n_P p_P > 2.62 n_T p_T$. The observed relationships between P and S and S and T events indicate that $n_P p_P > 1.81 n_S p_S$ and $n_S p_S > 1.55 n_T p_T$.

The CV also constrains the relationship between n and p

$$p \geq \frac{1}{1 + CV^2 n} \tag{B3}$$

where the equality holds for a simple binomial model and the inequality for a compound binomial model (where p is the mean of p_k). Even under these constraints, *Eqs.* B*2* and B*3* allow a wide range of physiologically reasonable n and p combinations consistent with the empirically observed PMs.

Appendix B3: extension to synchronized neurons

Considering N cells firing synchronously, where *cell* $i = 1, \ldots, N$ has n_i potential quanta for release, the total number n of possible quanta is

$$n = \sum_{i=1}^{N} n_i \tag{B4}$$

Denoting the probability of release of quantum k in cell i as $p_{k,i}$, then the mean number of quanta released is

$$m = \sum_{i=1}^{N} \sum_{k=1}^{n_i} p_{k,i} \tag{B5}$$

which is exactly the same as if all n quanta were from a single cell.

The variance in the number of quanta released in the N cells is

$$\sigma^2 = \sum_{i=1}^{N} \sum_{k=1}^{n_i} p_{k,i}(1 - p_{k,i}) \tag{B6}$$

which again is identical to the situation where all n quanta were from a single cell.

We thank D. Ruelle (Institut des Hautes Etudes Scientifiques), R. Miles (Institut Pasteur), D. S. Faber (Albert Einstein College of Medicine, NY), P. Rapp (Medical College of Pennsylvania), and K. Hatta for experimental support.

This work was supported by Office of Naval Research Grant N00014-97-0226.

Present address of D. Kaplan: Dept. of Mathematics, Macalester College, St. Paul, MN 55105.

REFERENCES

ABARBANEL HDI. *Analysis of Observed Chaotic Data.* New York: Springer-Verlag, 1995.

ABARBANEL HD, HUERTA R, RABINOVICH MI, RULKOV NF, ROWAT PF, AND SELVERSTON AI. Synchronized action of synaptically coupled chaotic model neurons. *Neural Comput* 8: 1567–1602, 1996.

ARIELI A, SHOHAM D, HILDESHEIM R, AND GRINVALD A. Coherent spatiotemporal patterns of ongoing activity revealed by real-time optical imaging coupled with single-unit recording in the cat visual cortex. *J Neurophysiol* 73: 2072–2093, 1995.

ARIELI A, STERKIN A, GRINVALD A, AND AERTSEN A. Dynamics of ongoing activity: explanation of the large variability in evoked cortical responses. *Science* 273: 1868–1871, 1996.

BORISYUK GN, BORISYUK RM, KHIBNIK AI, AND ROOSE D. Dynamics and bifurcations of two coupled neural oscillators with different connection types. *Bull Math Biol* 57: 809–840, 1995.

BRAGIN A, JANDO G, NADASDY Z, HETKE J, WISE K, AND BUZSAKI G. Gamma (40–100 Hz) oscillation in the hippocampus of the behaving rat. *J Neurosci* 15: 47–60, 1995.

BROCK L, COOMBS J, AND ECCLES J. The recording of potentials from motoneurones with an intracellular electrode. *J Physiol (Lond)* 117: 431–460, 1952.

BUZSAKI G, LLINAS R, SINGER W, AND BERTHOZ A. *Temporal Coding in the Brain.* New-York: Springer-Verlag, 1994.

CALVIN W AND STEVENS C. Synaptic noise as a source of variability in the interval between action potentials. *Science* 155: 842–844, 1967.

DEL CASTILLO J AND KATZ B. Quantal components of the end-plate potential. *J Physiol (Lond)* 124: 560–573, 1952.

ECKMANN J-P, KAMPHORST SO, AND RUELLE D. Recurrence plots of dynamical systems. *Europhys Lett* 4: 973–977, 1987.

EGGERMONT JJ. Is there a neural code? *Neurosci Biobehav Rev* 22: 355–370, 1998.

FABER DS AND KORN H. Electrophysiology of the Mauthner cell: basic properties, synaptic mechanism and associated networks. In: *Neurobiology of the Mauthner Cell*, edited by Faber DS and Korn H. New York: Raven, 1978, p. 47–131.

FABER DS AND KORN H. Transmission at a central inhibitory synapse. I. Magnitude of unitary postsynaptic conductance change and kinetics of channel activation. *J Neurophysiol* 48: 654–678, 1982.

FAURE P AND KORN H. A nonrandom dynamic component in the synaptic noise of a central neuron. *Proc Natl Acad Sci USA* 94: 6506–6511, 1997.

FAURE P AND KORN H. Temporal structures of synaptic noise and their relation with quantal release of neurotransmitter (Abstract). *Eur J Neurosci* 10: 415, 1998a.

FAURE P AND KORN H. A new method to estimate the Kolmogorov entropy from recurrence plots: its application to neuronal signals. *Physica D* 122: 265–279, 1998b.

FERSTER D. Is neural noise just a nuisance? *Science* 273: 1812, 1996.

FUJII H, ITO H, AIHARA K, ICHINOSE N, AND TSUKADA M. Dynamical cell assembly hypothesis—theoretical possibility of spatio temporal coding in the cortex. *Neural Network* 9: 1303–1350, 1996.

FURSHPAN EJ AND FURUKAWA T. Intracellular and extracellular responses of the several regions of the Mauthner cell of goldfish. *J Neurophysiol* 25: 732–771, 1962.

FURUKAWA T AND FURSHPAN EJ. Two inhibitory mechanisms in the Mauthner neurons of goldfish. *J Neurophysiol* 24: 140–176, 1963.

GARFINKEL A, SPANO ML, DITTO WL, AND WEISS JN. Controlling cardiac chaos. *Science* 257: 1230–1235, 1992.

GEORGOPOULOS AP, SCHWARTZ AB, AND KETTNER RE. Neuronal population coding of movement direction. *Science* 233: 1416–1419, 1986.

GIBSON JR, BEIERLEIN M, AND CONNORS BW. Two networks of electrically coupled inhibitory neurons in neocortex. *Nature* 402: 75–79, 1999.

GLASS L AND MACKEY MC. *From Clocks to Chaos*. Princeton, NJ: Princeton Univ. Press, 1988.

GUCKENHEIMER J AND ROWAT P. Dynamical analysis of real neuronal networks. In: *Neurons, Networks, and Motor Behavior*, edited by Stein PSG, Grillner S, Selverston AI, and Stuart DG. London, UK: MIT Press, 1997, p. 151–163.

HANSEL D AND SOMPOLINSKY H. Synchronization and computation in a chaotic neural network. *Phys Rev Lett* 68: 718–721, 1992.

HATTA K AND KORN H. Tonic inhibition alternates in paired neurons that set direction of fish escape reaction. *Proc Natl Acad Sci USA* 96: 12090–12095, 1999.

HEBB DO. *The Organisation of Behavior—A Neurophysiological Theory*. New York: Wiley, 1949.

HINDMARSH JL AND ROSE RM. A model of neuronal bursting using three coupled first order differential equations. *Proc R Soc Lond B Biol Sci* 221: 87–102, 1984.

HOPFIELD JJ. Pattern recognition computation using action potential timing for stimulus representation. *Nature* 376: 33–36, 1995.

JEFFERYS JG, TRAUB RD, AND WHITTINGTON MA. Neuronal networks for induced "40 Hz" rhythms. *Trends Neurosci* 19: 202–208, 1996.

KANTZ H AND SCHREIBER T. *Non Linear Time Series Analysis*. Cambridge, UK: Cambridge Univ. Press, 1997.

KEENER JP AND GLASS L. Global bifurcations of a periodically forced nonlinear oscillator. *J Math Biol* 21: 175–190, 1984.

KEENER J AND SNEYD J. *Mathematical Physiology*. New York: Springer, 1998.

KORN H AND FABER DS. Vertebrate central nervous system: same neurons mediate both electrical and chemical inhibitions. *Science* 194: 1166–1169, 1976.

KORN H AND FABER DS. Transmission at a central inhibitory synapse. IV. Quantal structure of synaptic noise. *J Neurophysiol* 63: 198–222, 1990.

KORN H AND FABER DS. Quantal analysis and synaptic efficacy in the CNS. *Trends Neurosci* 14: 439–445, 1991.

KORN H, FABER DS, BURNOD Y, AND TRILLER A. Regulation of efficacy at central synapses. *J Neurosci* 4: 125–130, 1984.

KORN H, FABER DS, AND TRILLER A. Probabilistic determination of synaptic strength. *J Neurophysiol* 55: 402–421, 1986.

KORN H, FABER DS, AND TRILLER A. Convergence of morphological, physiological, and immunocytochemical techniques for the study of single Mauthner cells. In: *Handbook of Chemical Neuroanatomy. Analysis of Neuronal Microcircuits and Synaptic Interactions*, edited by Björklund A, Hükfelt T,

Wouterlood FG, and van der Pol AN. Amsterdam: Elsevier, 1990, vol. 8, p. 403–480.

KORN H, MALLET A, TRILLER A, AND FABER DS. Transmission at a central inhibitory synapse. II. Quantal description of release, with a physical correlate for binomial n. *J Neurophysiol* 48: 679–707, 1982.

KORN H, ODA Y, AND FABER DS. Long-term potentiation of inhibitory circuits and synapses in the central nervous system. *Proc Natl Acad Sci USA* 89: 440–443, 1992.

KORN H, SOTELO C, AND BENNETT MVL. The lateral vestibular nucleus of the toadfish (*Opsanus tau*): ultrastructural and electrophysiological observations with special reference to electrotonic transmission. *Neuroscience* 2: 851–884, 1977.

MAINEN ZF AND SEJNOWSKI TJ. Reliability of spike timing in neocortical neurons. *Science* 268: 1503–1506, 1995.

MARTIN AR. A further study of the statistical composition of the endplate potential. *J Physiol (Lond)* 130: 114–122, 1955.

NICOLELIS MA, BACCALA LA, LIN RC, AND CHAPIN JK. Sensorimotor encoding by synchronous neural ensemble activity at multiple levels of the somatosensory system. *Science* 268: 1353–1358, 1995.

ODA Y, CHARPIER S, MURAYAMA Y, SUMA C, AND KORN H. Long-term potentiation of glycinergic inhibitory synaptic transmission. *J Neurophysiol* 74: 1056–1074, 1995.

ODA Y, KAWASAKI K, MORITA M, KORN H, AND MATSUI H. Inhibitory long-term potentiation underlies auditory conditioning of goldfish escape behaviour. *Nature* 394: 182–185, 1998.

PARZEN E. On estimation of a probability density function and mode. *Ann Math Stats* 33: 1065–1076, 1962.

PEI X AND MOSS F. Characterization of low-dimensional dynamics in the crayfish caudal photoreceptor. *Nature* 379: 618–621, 1996.

PERKEL DH AND BULLOCK TH. Neural coding. *Neurosci Res Prog Bull* 6: 221–348, 1968.

RAPP PE, ALBANO AM, SCHMAH TI, AND FARWELL LA. Filtered noise can mimic low dimensional chaotic attractors. *Phys Rev E* 47: 2289–2297, 1993.

REDMAN S. Quantal analysis of synaptic potentials in neurons of the central nervous system. *Physiol Rev* 70: 165–198, 1990.

RIEHLE A, GRUN S, DIESMANN M, AND AERTSEN A. Spike synchronization and rate modulation differentially involved in motor cortical function. *Science* 278: 1950–1953, 1997.

RINZEL J, TERMAN D, WANG X, AND ERMENTROUT B. Propagating activity patterns in large-scale inhibitory neuronal networks. *Science* 279: 1351–1355, 1998.

ROSE RM AND HINDMARSH JL. A model of a thalamic neuron. *Proc R Soc Lond B Biol Sci* 225: 161–193, 1985.

SCHIFF SJ, JERGER K, DUONG DH, CHANG T, SPANO ML, AND DITTO WL. Controlling chaos in the brain. *Nature* 8: 615–620, 1994.

SCHREIBER T. Interdisciplinary application of nonlinear time series methods. *Phys Rep* 308: 1–64, 1999.

SCHREIBER T AND SCHMITZ A. Improved surrogate data for nonlinearity tests. *Phys Rev Lett* 77: 635–638, 1996.

SCHREIBER T AND SCHMITZ A. Surrogate time series. *Physica D* 142: 346–382, 2000.

SHADLEN MN AND NEWSOME WT. Noise, neural codes and cortical organization. *Curr Opin Neurobiol* 4: 569–579, 1994.

SHADLEN MN AND NEWSOME WT. Is there a signal in the noise? *Curr Opin Neurobiol* 5: 248–250, 1995.

SHADLEN MN AND NEWSOME WT. The variable discharge of cortical neurons: implications for connectivity, computation, and information coding. *J Neurosci* 18: 3870–3896, 1998.

SHERMAN A AND RINZEL J. Rhythmogenic effects of weak electrotonic coupling in neuronal models. *Proc Natl Acad Sci USA* 89: 2471–2474, 1992.

SINGER W. Synchronization of cortical activity and its putative role in information processing and learning. *Annu Rev Physiol* 55: 349–374, 1993.

SKARDA CA AND FREEMAN WJ. How brain make chaos in order to make sense of the world. *Behav Brain Sci* 10: 161–195, 1987.

SKARDA CA AND FREEMAN WJ. Chaos and the new science of the brain. *Concepts Neurosci* 1: 275–285, 1990.

SO P, FRANCIS JT, NETOFF TI, GLUCKMAN BJ, AND SCHIFF SJ. Periodic orbits: a new language for neuronal dynamics. *Biophys J* 74: 2776–2785, 1998.

SOFTKY W. Simple codes versus efficient codes. *Curr Opin Neurobiol* 5: 239–247, 1995.

SOFTKY WR AND KOCH C. The highly irregular firing of cortical cells is inconsistent with temporal integration of random EPSPs. *J Neurosci* 13: 334–350, 1993.

STEVENS CF AND ZADOR AM. Input synchrony and the irregular firing of cortical neurons. *Nat Neurosci* 1: 210–217, 1998.

THEILER J, EUBANK S, LONGTIN A, GALDRIKIAN B, AND FARMER JD. Testing for nonlinearity in time series: the method of surrogate data. *Phys D* 58: 77–94, 1992.

TRAUB RD, WHITTINGTON MA, STANFORD IM, AND JEFFERYS JG. A mechanism for generation of long-range synchronous fast oscillations in the cortex. *Nature* 383: 621–624, 1996.

TRILLER A AND KORN H. Morphologically distinct classes of inhibitory synapses arise from the same neurons: ultrastructural identification from crossed vestibular interneurons intracellularly stained with HRP. *J Comp Neurol* 203: 131–155, 1981.

VAN VREESWIJK C AND SOMPOLINSKY H. Chaos in neuronal networks with balanced excitatory and inhibitory activity. *Science* 274: 1724–1726, 1996.

VON DER MALSBURG C. *The Correlation Theory of Brain Function.* Internal Report, Max Planck Institute for Biophysical Chemistry, Goettingen, Germany. 1981.

WEBBER CL AND ZBILUT JP. Dynamical assessment of physiological systems and states using recurrence plot strategies. *J Appl Physiol* 76: 965–973, 1994.

WHITE JA, CHOW CC, RITT J, SOTO-TREVINO C, AND KOPELL N. Synchronization and oscillatory dynamics in heterogeneous, mutually inhibited neurons. *J Comput Neurosci* 5: 5–16, 1998.

WHITTINGTON MA, TRAUB RD, AND JEFFERYS JG. Synchronized oscillations in interneuron networks driven by metabotropic glutamate receptor activation. *Nature* 373: 612–615, 1995.

WILSON MA AND BOWER JM. The simulation of Large-Scale Neural Networks. In: *Methods in Neuronal Modeling, From Synapses to Networks*, edited by Koch C and Segev I. Cambridge, MA: MIT, 1989, p. 291–334.

ZADOR A. Impact of synaptic unreliability on the information transmitted by spiking neurons. *J Neurophysiol* 79: 1219–1229, 1998.

ZOTTOLI A. Correlation of the startle reflex and Mauthner cell auditory responses in unrestrained goldfish. *J Exp Biol* 66: 243–254, 1977.